npj | climate and atmospheric science

Article

Published in partnership with CECCR at King Abdulaziz University

https://doi.org/10.1038/s41612-024-00881-1

Simulated Antarctic sea ice expansion reconciles climate model with observation

Wei Liu ✉

Observations reveal Antarctic sea ice expansion and Southern Ocean surface cooling trends from 1979 to 2014, whereas climate models mostly simulate the opposite. Here I use historical ensemble simulations with multiple climate models to show that sea-ice natural variability enables the models to simulate an Antarctic sea ice expansion during this period under anthropogenic forcings. Along with sea-ice expansion, Southern Ocean surface and subsurface temperatures up to 50°S, as well as lower tropospheric temperatures between 60°S and 80°S, exhibit significant cooling trends, all of which are consistent with observations. Compared to the sea-ice decline scenario, Antarctic sea ice expansion brings tropical precipitation changes closer to observations. Neither the Southern Annular Mode nor the Interdecadal Pacific Oscillation can fully explain the simulated Antarctic sea ice expansion over 1979–2014, while the sea-ice expansion is closely linked to surface meridional winds associated with a zonal wave 3 pattern.

Since the satellite era, Antarctic sea ice area has exhibited a slight but significant increase trend over three to four decades[1] (also see Fig. 1a, and Methods). The Antarctic sea ice increases were attributed to Antarctic glacial melt[2–4] and changes in the Southern Annular Mode (SAM)[5] triggered by anthropogenic greenhouse gas increases and stratospheric ozone depletion, despite the latter mechanism being argued by ref. 6. Antarctic sea ice increases could also be related to internal climate variability such as tropical Pacific variability[7,8] including the Interdecadal Pacific Oscillation (IPO)[9], Atlantic Multidecadal Variability[10] and the natural variability of Southern Ocean convection[11]. Nonetheless, Antarctic sea ice extent diminished abruptly in 2016[12] and appeared to enter a rapid decline stage thereafter[13]. In contrast to this sea ice decline, the earlier Antarctic sea ice expansion appears elusive in the context of anthropogenetic warming, and thus forms the focus on this study.

Along with the expansion of Antarctic sea ice, sea surface temperatures (SSTs) in the broad Southern Ocean displayed a slight but significant cooling trend during the same period[11,14,15] (also see Fig. 2a and Fig. S1a). This surface cooling trend has been attributed to freshwater input from Antarctic ice-sheet melt[2–4], Southern Ocean heat transport by meridional overturning circulation[14,16], ocean convection induced natural variability[11], and surface westerly wind change caused by the trend of the SAM via altering the northward Ekman transport[5], despite the last mechanism being argued by ref. 17. The Southern Ocean SST cooling is potentially linked to the tropical southeast Pacific cooling[7,18] via atmospheric teleconnections[19] and cloud feedback[20]. Nevertheless, it remains challenging for state-of-art climate models to reproduce the observed Antarctic sea ice expansion and Southern Ocean surface cooling prior to 2016. Most models under historical climate forcings, instead, simulate a reduction in Antarctic sea ice cover[21,22] and a warming SST trend over the Southern Ocean[7,15]. These model-observation discrepancies cast doubt on the confidence of model projections in the current and future centuries as well as model estimates of climate sensitivity[23].

Efforts thus have been made for allowing coupled climate models to reproduce the observed Antarctic sea ice expansion, which include wind nudging by imposing the observed large-scale circulation in the atmosphere[24], inputting anomalous freshwater into the Southern Ocean to mimic the meltwater from Antarctic ice sheets[25], a combination of the previous two methods[26], corrections of sea ice drift velocity[27], high-resolution modelling[28] and restoring Southern Ocean SSTs to observations[18]. Many of these approaches, however, introduce observational constraints on atmosphere circulation or SST, potentially interfering with the natural atmosphere-ice-ocean coupling in model. In this context, critical scientific questions naturally arise: Will a simulated Antarctic sea ice expansion render the Southern Ocean surface cool, or the other way around, given ice-ocean coupling? Or more specifically, to what extent can the bias of Antarctic sea ice trend account for the bias of Southern Ocean SST trend during the three to four decades since the satellite era? In addition, how will the Antarctic sea ice expansion associate with other components of Earth's climate system? To address these scientific questions, here I investigate historical ensemble simulations with Coupled Model Intercomparison Project phase 5/6 (CMIP5/6) climate models. I will show that, a subset of CMIP5/6 ensemble simulations can successfully reproduce the observed Antarctic sea ice expansion from 1979 to 2014 due mainly to natural variability of sea ice, demonstrating that natural variability alone can

Department of Earth and Planetary Sciences, University of California Riverside, Riverside, CA, USA. ✉e-mail: wei.liu@ucr.edu

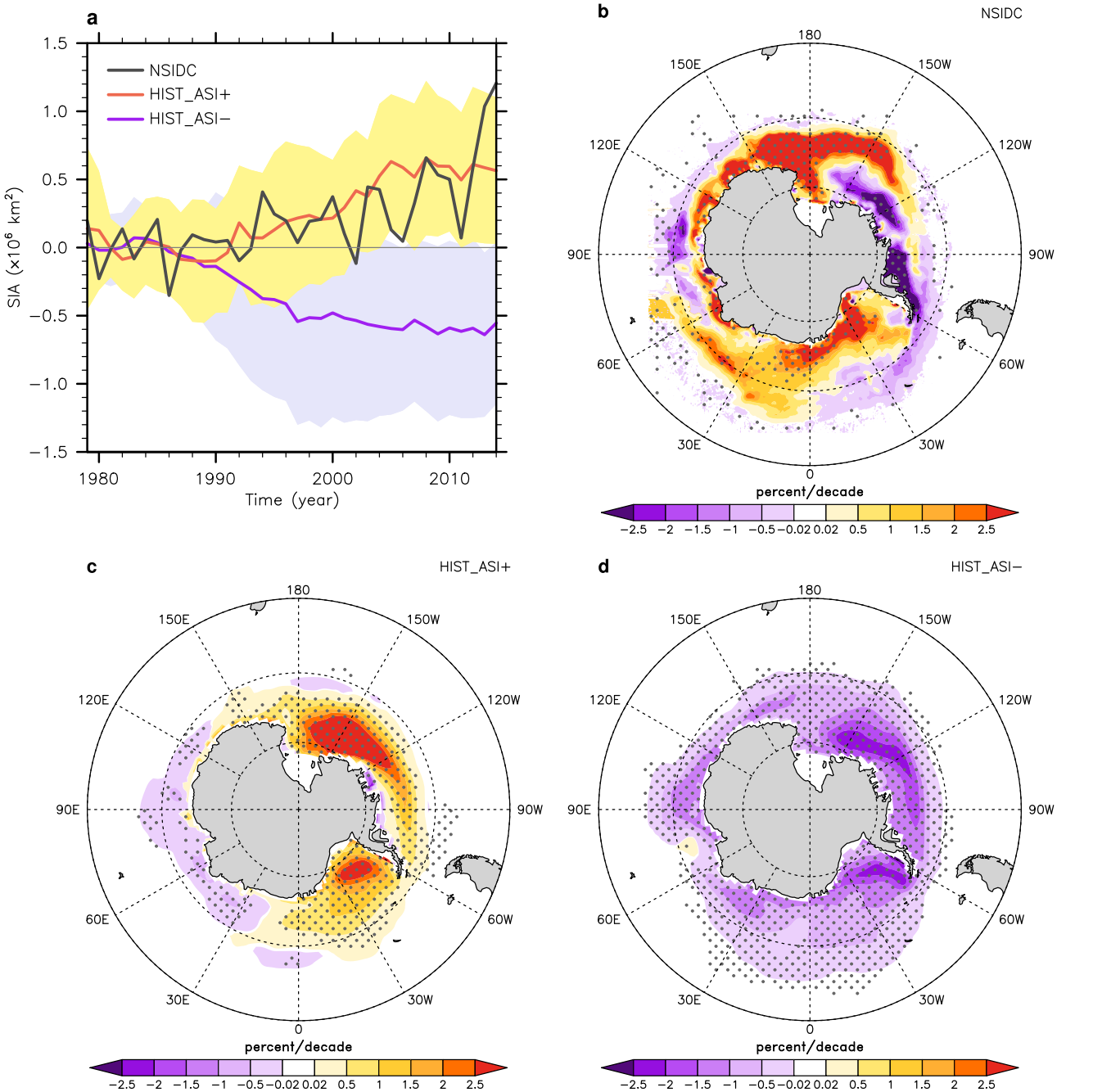

Fig. 1 | Observed and simulated changes in Antarctic sea ice. a Anomalies (relative to the 1979-1988 average) of the total annual mean Antarctic sea ice area from NSIDC observations (black), HIST_ASI+ (ensemble mean, red; ensemble spread, yellow), and HIST_ASI- (ensemble mean, purple; ensemble spread, light purple). The ensemble spread in HIST_ASI+ or HIST_ASI- is calculated as one standard deviation among ensembles. **b**–**d** Annual mean sea ice concentration trends over 1979–2014 (color shading in percent/decade) for (**b**) NSIDC observations, (**c**) HIST_ASI+ and (**d**) HIST_ASI- ensemble means. The stipples refer to the regions where trends are statistically significant based on Student's t-test at 95% confidence level.

generate multidecadal periods of Antarctic sea ice expansion even with greenhouse gas warming[29], which aligns with the findings that observed sea ice area trends during this period lie well within the range of natural variability of CMIP5/6 pre-industrial controls[22,30]. More importantly, these simulations elucidate the changes along with increased Antarctic sea ice in a natural atmosphere-ice-ocean coupled system, which is distinct from previous studies.

Results

I leverage six CMIP5/6 climate models (see Methods, and Table S1) whose historical simulations exhibit large diversity among ensembles due to internal climate variability. Between 1979 and 2014, there are 24 ensembles (the HIST_ASI+ group, thereafter, see Methods) simulating a significant ($p < 0.05$) annual mean Antarctic sea ice expansion at a rate of 0.22 ± 0.17 million km^2/decade (ensemble mean ± one standard derivation among ensembles), aligning with the observed sea ice increasing trend (0.21 million km^2/decade, Fig. 1a) during this period. Both observations and HIST_ASI+ ensemble mean show significant sea ice increases in the Weddle and Ross Seas. While differences still exist between the two such as those in the Cosmonaut Sea, where sea ice expands in observations but dwindles in HIST_ASI+ (Fig. 1b, c), which might relate to different surface wind fluctuations that redistribute the sea ice in the region. On the other hand, 53

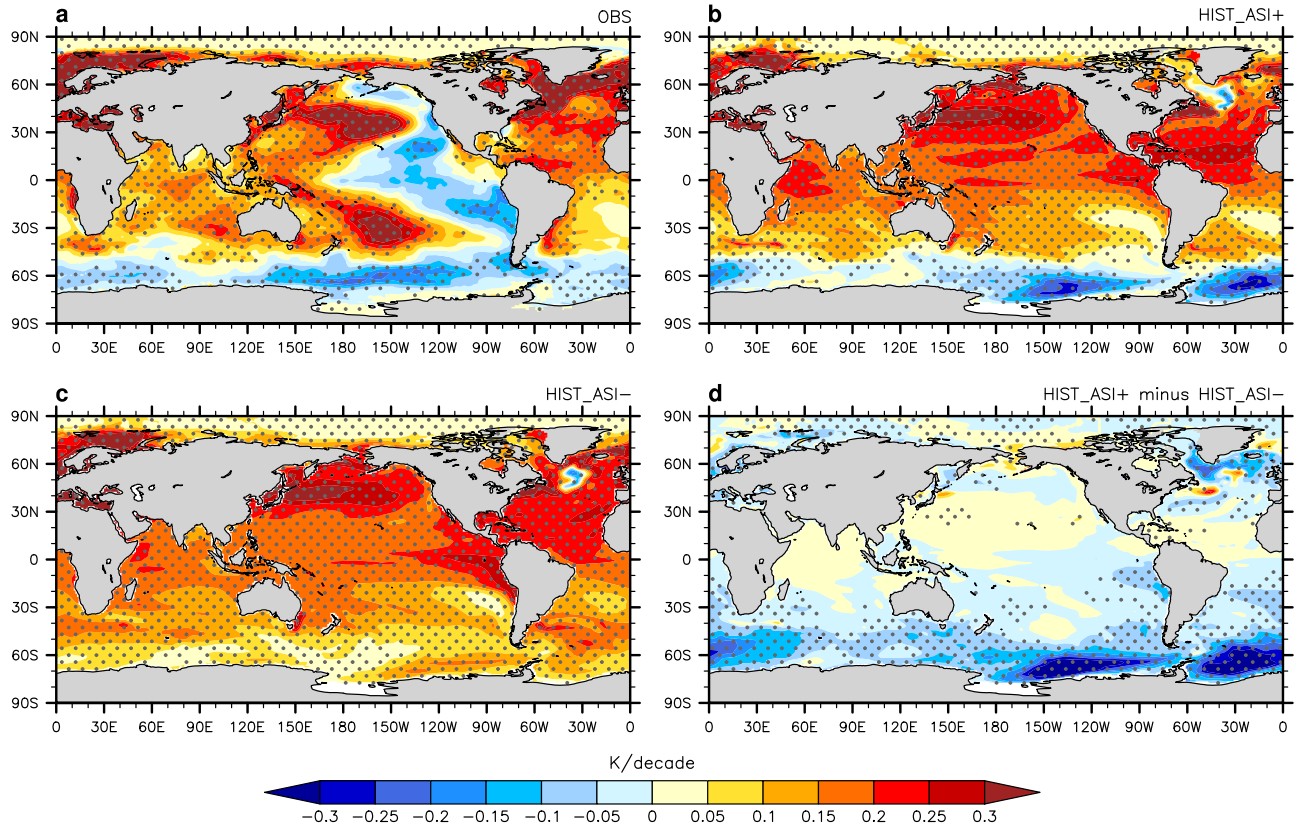

Fig. 2 | Observed and simulated changes in sea surface temperature. Linear trends of annual mean sea surface temperature over 1979–2014 (color shading in K/decade) from (**a**) the average of COBESSTv2, ERSSTv5 and HadISST, (**b**) HIST_ASI+ and (**c**) HIST_ASI- ensemble means as well as (**d**) the difference between the two (HIST_ASI+ minus HIST_ASI-). The stipples refer to the regions where trends are statistically significant based on Student's t-test at 95% confidence level.

ensembles (the HIST_ASI- group thereafter) present a significant ($p < 0.05$) decline trend of annual mean Antarctic sea ice area at a rate of -0.23 ± 0.21 million km^2/decade (ensemble mean ± one standard derivation among ensembles) over 1979-2014 (Fig. 1a), consistent with previous CMIP5 and CMIP6 simulations[21,22] but opposite to observations. HIST_ASI- ensemble mean simulates a general reduction in sea ice concentration around Antarctica (Fig. 1d).

The expansion of Antarctic sea ice in HIST_ASI+ is linked to a significant cooling of annual mean SST (Fig. 2b) and surface air temperature (SAT, Fig. S1b) primarily to the south of around 50°S in the Southern Ocean, which resembles observations (see Methods, Fig. 2a and Fig. S1a) but differs from the general Southern Ocean SST and SAT warming in HIST_ASI- (Fig. 2c and Fig. S1c). This finding suggests that the Antarctic sea ice expansion between 1979 and 2014 is primarily related to Southern Ocean SST and SAT cooling up to around 50°S, with little implication for further north. The observed SST and SAT cooling north of 50°S (Fig. 2a and Fig. S1a), on the other hand, could be associated with factors such as tropical Pacific variability[8,9]. This is because HIST_ASI+ ensembles do not capture the same phase change in observed tropical Pacific variability like the IPO from 1979 to 2014. Nonetheless, the ensemble-mean difference between HIST_ASI+ and HIST_ASI- reveals strong negative SST trends not only across the Southern Ocean but also in the tropical south Pacific and south Atlantic (Fig. 2d), implying teleconnections between the Southern and tropical oceans[18–20]. This result further indicates that, when compared to retreating ice, Antarctic sea ice expansion has a cooling effect on tropical Pacific and Atlantic SST, but it is insufficient to offset the background anthropogenic warming or modelled tropical climate variability. Thereby, unlike observations, HIST_ASI+ ensemble mean simulates a weak tropical warming from 1979 to 2014. It is also worth noting that, aside from the Southern and tropical oceans, the ensemble-mean difference between HIST_ASI+ and HIST_ASI- exhibits anomalous surface cooling trends over the subpolar North Pacific and Atlantic (Fig. 2d), and mid- to high latitude Europe, Asia and North America (Fig. S1d), indicative of teleconnections caused by Antarctic sea ice change over a global scale.

Beyond the surface, the expansion of Antarctic sea ice in either observations (see Methods) or HIST_ASI+ ensemble mean is accompanied by a significant subsurface cooling off the Antarctic coast to about 50°S, mostly in the upper 100 m, and enhanced warming beneath (Fig. 3a, b). This is perhaps due to a net northward sea-ice transport that allows freshwater to be extracted near Antarctica and released into the open ocean, intensifying stratification and thus cooling the surface open-ocean waters while reducing vertical mixing to warm the waters beneath[31]. Cooling in the upper-layer waters, in turn, can aid in the expansion of sea ice[32]. Significant subsurface cooling is absent in HIST_ASI- ensemble mean, instead, a consistent subsurface warming trend prevails in the Southern Ocean from 1979 to 2014 (Fig. 3c). The ensemble-mean difference between HIST_ASI+ and HIST_ASI- illustrates a conspicuous cooling trend in the upper 200 m across the entire Southern Ocean. At some latitudes, water cooling can reach as deep as 1000 m (Fig. 3d).

Besides the ocean, Antarctic sea ice expansion affects the atmosphere (Fig. 4). Although both HIST_ASI+ and HIST_ASI- ensembles can simulate the observed (see Methods) "tug of war" pattern of upper-troposphere tropical warming and amplified Arctic surface warming from 1979 to 2014 (Fig. 4a, c, e), their temperature changes differ in the Southern Hemisphere. Between 60°S and 80°S, HIST_ASI+ ensemble mean presents a significant tropospheric cooling from the surface to 700 hPa (Fig. 4c), which is present in observations (Fig. 4a). This pattern, however, is not represented by HIST_ASI- ensemble mean (Fig. 4e). Likewise, both observations (Fig. 4b) and HIST_ASI+ ensemble mean (Fig. 4d) witness a dipole-like change in zonal winds with positive and negative anomalies to the north and south of around 65°S, whilst this dipole-like wind change is less striking seen from the counterpart of HIST_ASI- (Fig. 4f). The

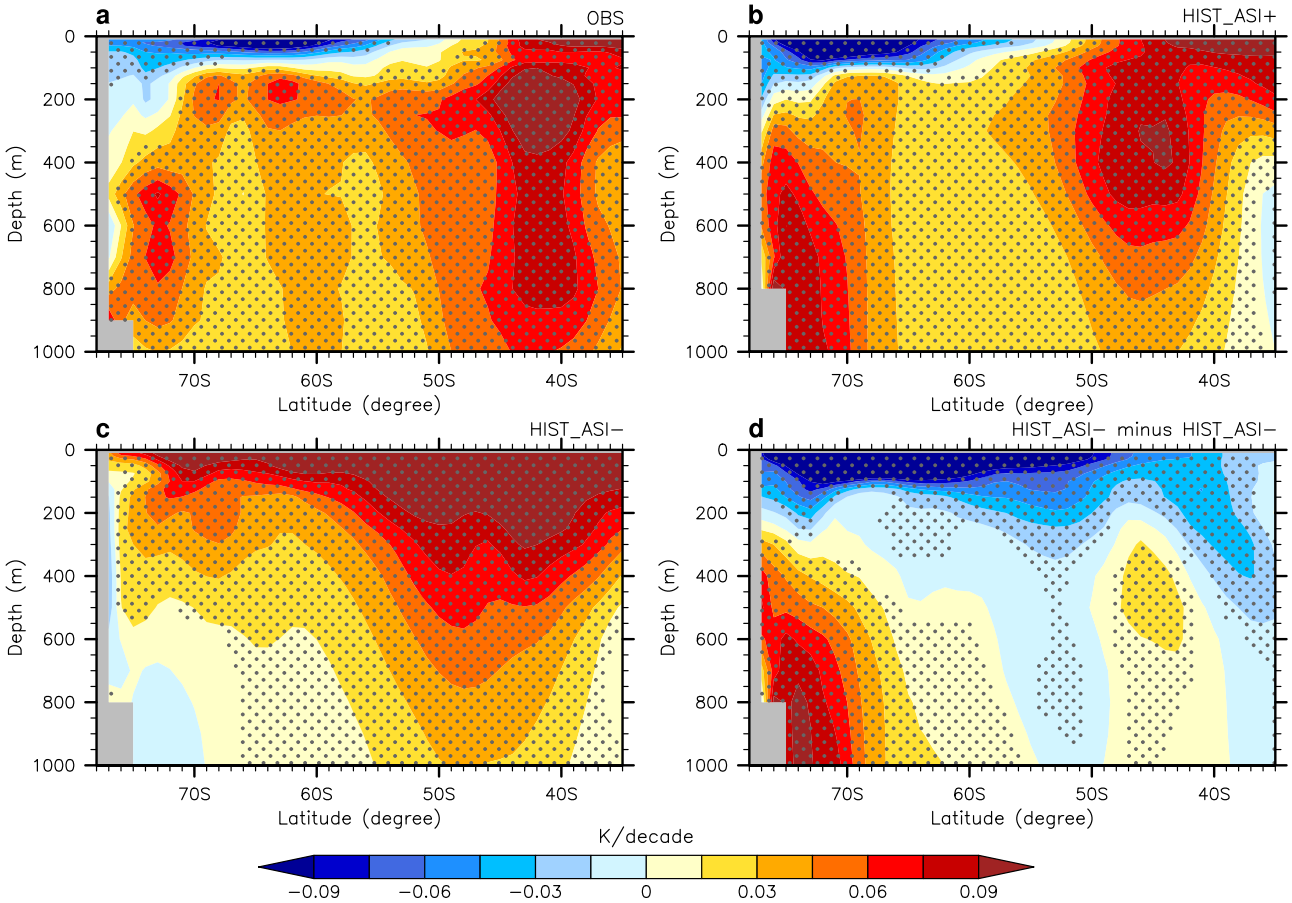

Fig. 3 | Observed and simulated changes in Southern Ocean temperature. Linear trends of zonal and annual mean ocean temperature in the upper 1000 m in the Southern Ocean over 1979–2014 (color shading in K/decade) from (**a**) the average of EN4, IAP and Ishii data, (**b**) HIST_ASI+ and (**c**) HIST_ASI- ensemble means as well as (**d**) the difference between the two (HIST_ASI+ minus HIST_ASI-). The stipples refer to the regions where trends are statistically significant based on Student's t-test at 95% confidence level.

ensemble-mean difference between HIST_ASI+ and HIST_ASI- unravels the linkage between Antarctic sea ice expansion and atmospheric cooling from 85°S to 20°S and from the surface to 500 hPa (Fig. 4g). As atmospheric temperatures alter, the winds on the poleward flank of the upper-level Southern Hemisphere subtropical westerlies intensify (Fig. 4h), meaning that Antarctic sea ice expansion can effectively displace the Southern Hemisphere westerly jets poleward.

The atmospheric influence of Antarctic sea ice expansion is not limit to temperature and zonal winds but extends to tropical precipitation[33] (Fig. 5). During 1979–2014, observations (see Methods) feature a dipole-like precipitation change with increases and decreases in the western and central tropical Pacific (Fig. 5a), whilst HIST_ASI- ensemble mean depicts a precipitation increase across the equatorial Pacific (Fig. 5c), in line with previous model results[34] but at odds with observations. HIST_ASI+ ensemble mean, on the other hand, simulates a dipole-like precipitation change that is closer to observations, despite the fact that the central Pacific precipitation decrease is weaker and farther south than observed (Fig. 5b). Interestingly, the ensemble-mean difference between HIST_ASI+ and HIST_ASI- reveals a dipole-like tropical precipitation pattern similar to observations (Fig. 5d), implying that Antarctic sea ice expansion plays a role in the change in tropical precipitation over 1979–2014.

The ensemble-mean difference in the zonal mean precipitation trend between HIST_ASI+ and HIST_ASI- further emphasizes the importance of Antarctic sea ice expansion (Fig. 6a). It shows a decrease and increase in annual mean precipitation to the south and north of about 5°N, indicating a trend of northward shift of the global zonal mean Intertropical Convergence Zone (ITCZ) due to Antarctic sea ice expansion over 1979–2014. Such ITCZ change can be explained using the atmospheric energy-flux theory[35–40] (see Methods), which describes an anti-correlation between the zonal mean ITCZ location and atmospheric cross-equatorial energy transport. The northward ITCZ migration, in particular, corresponds to an enhanced southward atmospheric cross-equatorial energy transport caused by changes in inter-hemispheric asymmetry of top of atmosphere (TOA) radiation and surface energy fluxes. Compared to their counterparts in the Northern Hemisphere, TOA radiation and surface energy fluxes between 60°S and 80°S in the Southern Hemisphere exhibit a larger amplitude change (Fig. 6c). Antarctic sea ice expansion reduces the net TOA shortwave radiation over 40–80°S, which, while partially offset by changes in the net longwave radiation (Fig. 6b), results in a decrease in the net downward TOA radiation at these latitudes. Meanwhile, sea ice expansion effectively promotes an anomalous downward surface energy flux from 60°S to 80°S, primarily in the form of turbulent (sensible and latent) heat fluxes (Fig. 6d). Compared to the ice retreat case in HIST_ASI-, sea-ice expansion in HIST_ASI+ modifies the temperature contrast between 2 m air temperature and surface temperature within 60–80°S (Fig. 6e), leading to an anomalous downward turbulent heat flux into ocean via sea ice. To summarize, Antarctic sea ice expansion abates the atmospheric moist static energy between 60°S and 80°S by reducing the net incoming radiation energy and promoting energy leakage through the surface (Fig. 6c), which contributes to an anomalous southward atmospheric cross-equatorial energy transport and hence a northward ITCZ shift.

Discussion

I then delve into the factors that may influence Antarctic sea ice variability as reflected by the difference between HIST_ASI+ and

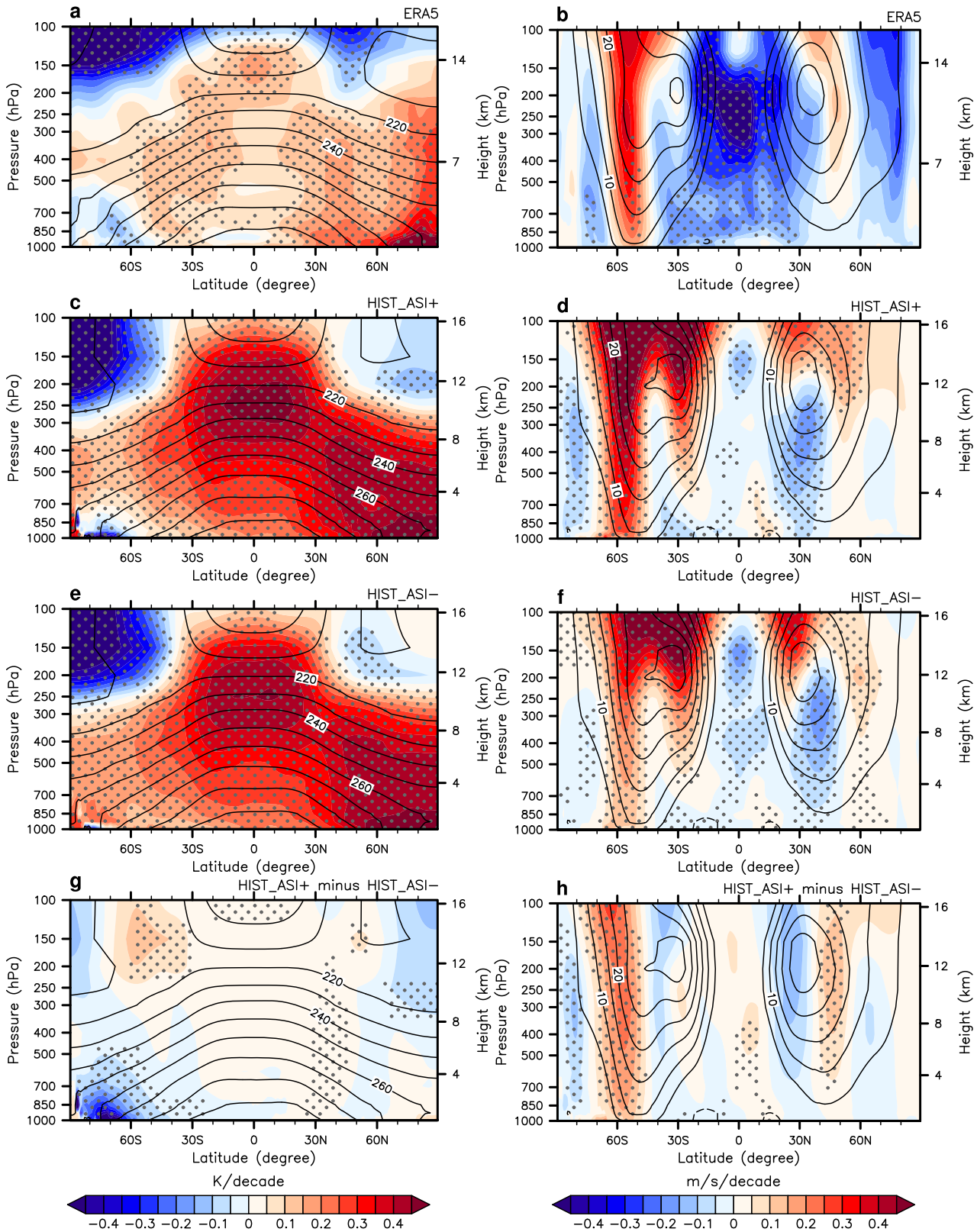

Fig. 4 | Observed and simulated changes in atmospheric temperature and zonal wind. a, **c**, **e**, **g** Linear trends of zonal and annual mean atmospheric temperature over 1979–2014 (color shading in K/decade) from (**a**) ERA5 reanalysis, (**c**) HIST_ASI+ and (**e**) HIST_ASI- ensemble means as well as (**g**) the difference between the two (HIST_ASI+ minus HIST_ASI-). Contours (in K) in (**a**, **c**, **e**) denote their annual mean climatology patterns during this period. Contours (in K) in (**g**) denote of HIST_ASI- annual mean climatology. The stipples refer to the regions where trends are statistically significant based on Student's t-test at 95% confidence level. **b**, **d**, **f**, **h** Same as (**a**, **c**, **e**, **g**) but for linear trends of zonal and annual mean zonal winds (shading in m/s/decade) and annual mean climatology of zonal winds (contour in m/s).

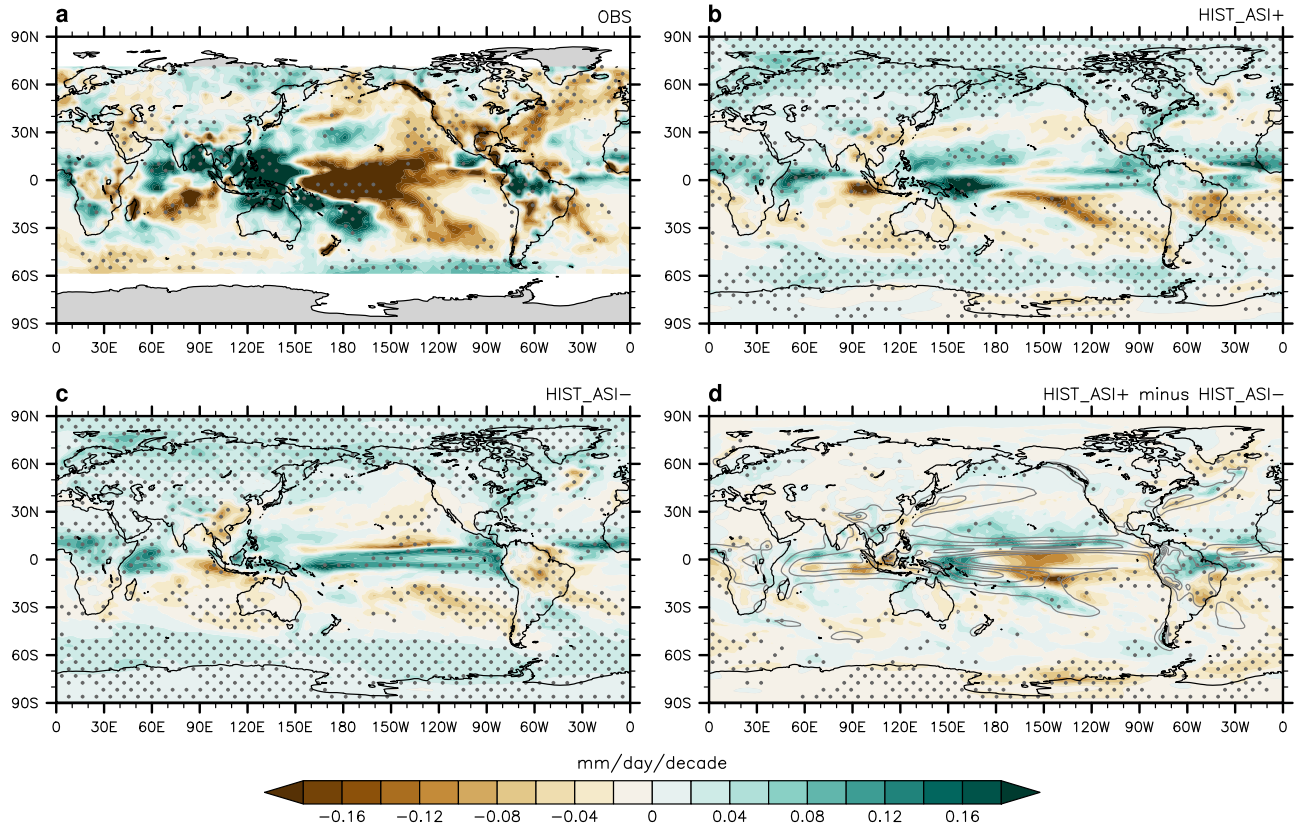

Fig. 5 | Observed and simulated changes in precipitation. Linear trends of annual mean precipitation over 1979–2014 (color shading in mm/day/decade) from (**a**) the average of CMAP, GPCP v2.3 and NOAA's Precipitation Reconstruction (PREC) data, (**b**) HIST_ASI+ and (**c**) HIST_ASI- ensemble means as well as (**d**) the difference between the two (HIST_ASI+ minus HIST_ASI-), superposed by annual mean precipitation climatology over 1979–2014 for HIST_ASI- ensemble mean (contour in mm/day with an interval of 2 mm/day). The stipples refer to the regions where trends are statistically significant based on Student's t-test at 95% confidence level.

HIST_ASI-. I first look into the SAM (see Methods) and discover that both HIST_ASI+ and HIST_ASI- simulate the December-January-February (DJF) SAM shifting toward a higher index state, as consistent with observations (Fig. 7a) and earlier studies[41,42]. From 1979 to 2014, the simulated trends of DJF SAM index (see Methods) by HIST_ASI+ and HIST_ASI- are 0.34 ± 0.20 SAM/decade and 0.23 ± 0.21 SAM/decade (ensemble mean ± one standard derivation among ensembles), respectively (Fig. 7b), both of which are within the observational range (from 0.35 SAM/decade in ERA5 to 0.58 SAM/decade in HadSLP2). Additionally, I examine the IPO during 1979–2014, and find that the observed (see Methods) IPO phase transition from positive before 1998 to negative after 1998 (Fig. 7c) cannot be captured by either the HIST_ASI+ or HIST_ASI- ensemble mean. This is a common modeling problem that has been identified by previous studies on the global warming hiatus[43]. In brief, neither the SAM[44] nor the IPO appear to be capable of adequately accounting for the difference in Antarctic sea ice trend between the ensemble means of HIST_ASI+ and HIST_ASI-.

I further probe the trends of near-surface (10-m) meridional wind over 1979–2014 in observations (see Methods), HIST_ASI+ and HIST_ASI-. Observations show northward wind trends over the Amundsen, Ross, Dumont D'Urville, Cosmonaut and King Håkon Seas (Fig. 8a), which could drive northward sea-ice drifts and thus sea ice expansion in these regions[45–47]. Likewise, albeit with detail differences, the HIST_ASI+ ensemble mean simulates northward wind trends in most of the above regions as observed, especially over the area between the Ross and Amundsen Seas (Fig. 8b), whereas the HIST_ASI- ensemble mean simulates less robust northward wind trends than that in HIST_ASI+ (Fig. 8c). The ensemble-mean difference between HIST_ASI+ and HIST_ASI- depicts a robust zonal wave 3 (ZW3)[48] like pattern (Fig. 8d), which was considered important to variability in sea ice extent[44,49]. This finding suggests that Antarctic sea ice expansion can be potentially attributed to near-surface meridional winds associated with the ZW3 pattern.

Conclusion

The current study reveals that a subset of CMIP5/6 historical ensemble simulations can reproduce the observed increase in Antarctic sea ice between 1979 and 2014. Because of sea-ice variability, these CMIP models are able to naturally simulate an Antarctic sea ice expansion over 1979–2014 in a group of ensembles under historical anthropogenic forcings, in contrast to earlier model experiments that interfered with the natural atmosphere–ice–ocean coupling for sea ice expansion. The simulated Antarctic sea-ice increase reconciles the models with observations from the perspectives of significant cooling trends in SST, SAT, subsurface ocean temperatures in the upper 100 m up to about 50°S in the Southern Ocean, and tropospheric temperatures from the surface to 700 hPa between 60°S and 80°S. During 1979–2014, the Antarctic sea ice expansion ensembles exhibit a precipitation trend in a dipole-like pattern with increased and decreased precipitation in the western and central tropical Pacific, respectively, which is more in line with observation when compared to the Antarctic sea ice decline ensembles. In a zonal-mean view, Antarctic sea ice expansion prompts a northward ITCZ displacement by creating an anomalous southward atmospheric cross-equatorial energy transport owing primarily to reduced atmospheric moist static energy between 60°S and 80°S. Furthermore, neither the SAM nor the IPO can be identified to fully interpret the simulated Antarctic sea ice expansion from 1979 to 2014. By contrast, the Antarctic sea ice expansion is inherently linked to near-surface meridional winds associated with the ZW3 pattern.

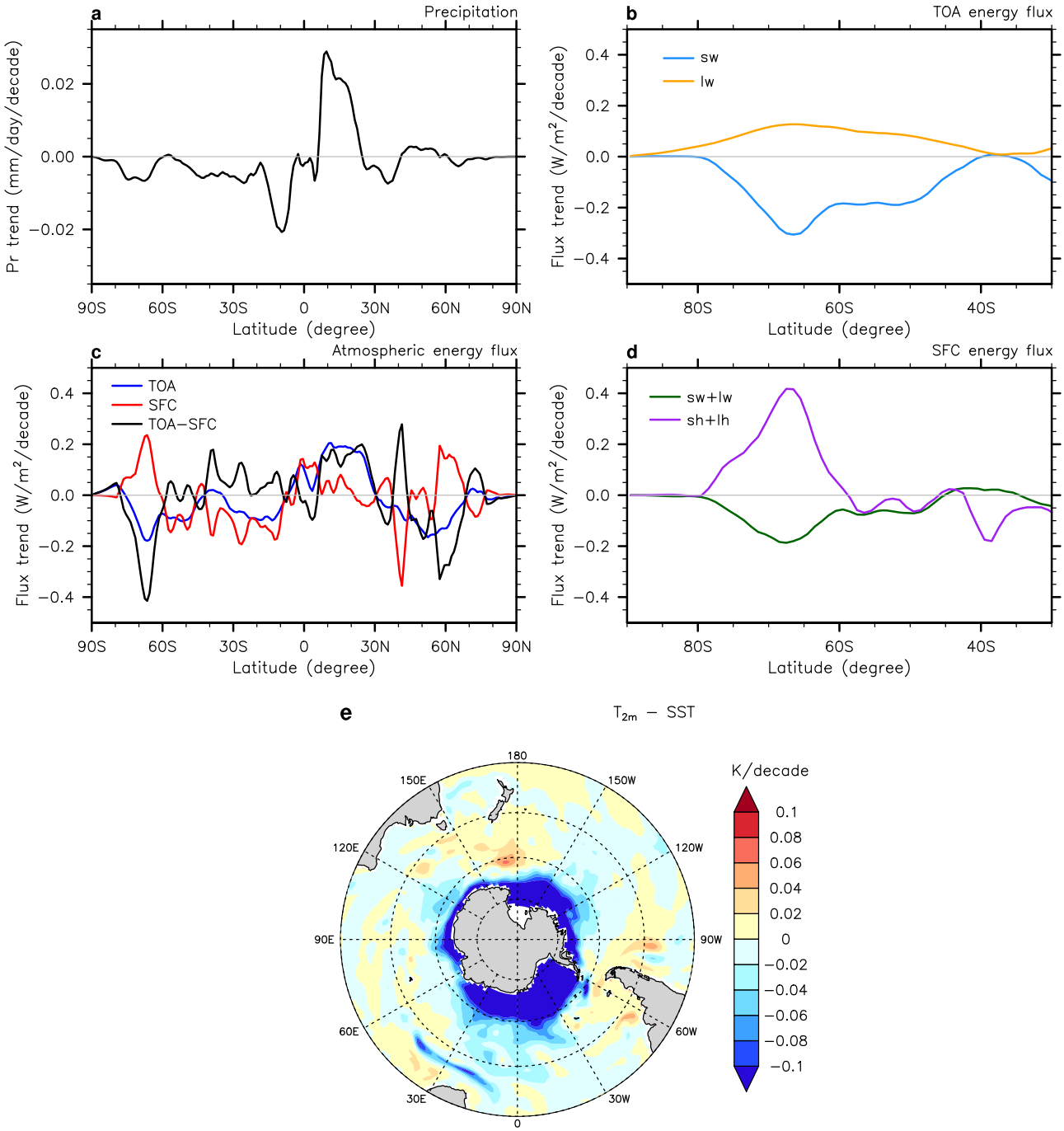

Fig. 6 | Effects of Antarctic sea ice change on zonal mean precipitation and energy fluxes. Linear trends of zonal and annual mean (**a**) precipitation, (**b**) the net TOA radiation energy flux (shortwave, medium blue; longwave, orange; both downward positive), (**c**) energy fluxes (the net TOA radiation, blue; the net surface energy flux, red; TOA minus surface, black; all downward positive), (**d**) surface energy flux (shortwave plus longwave radiation, green; turbulent sensitive plus latent heat flux, purple; both downward positive). **e** Map of temperature contrast (2-m air temperature minus sea surface temperature) trend over 1979–2014 (shading in K/decade) for the difference between HIST_ASI+ and HIST_ASI- ensemble means (HIST_ASI+ minus HIST_ASI-). A weight of cosine of latitude has been applied to (**a**–**d**).

Methods

Observations

I use passive microwave monthly Southern Hemisphere sea ice concentration data by NASA Team algorithm[50] processed by the National Snow and Ice Data Center (NSIDC), which are gridded on the NSIDC polar stereographic grid with 25 km × 25 km grid cells. I examine annual mean values of sea ice concentration and total sea ice area from 1979 to 2014. I employ the metric of sea ice area here, since I target observation-model comparison, and this metric is independent of model grid and resolution.

I exploit COBE-SSTv2, ERSSTv5 and HadISST data[51–53] between 1979 and 2014 to investigate the observed SST trend during this period. I use their average to reduce the uncertainty of the observation. All three sets of data are collected monthly. COBE-SSTv2 and HadISST data have a horizontal resolution of 1°, while ERSSTv5 data have a horizontal resolution of 2°. To measure the IPO, I calculate the Tripole Index (TPI) using these three data sets, which is defined as the difference between the SST anomaly (SSTA) averaged over the central equatorial Pacific and the average of the SSTA in the Northwest and Southwest Pacific[54] and based on the climatology time period of January 1979 to December 2014.

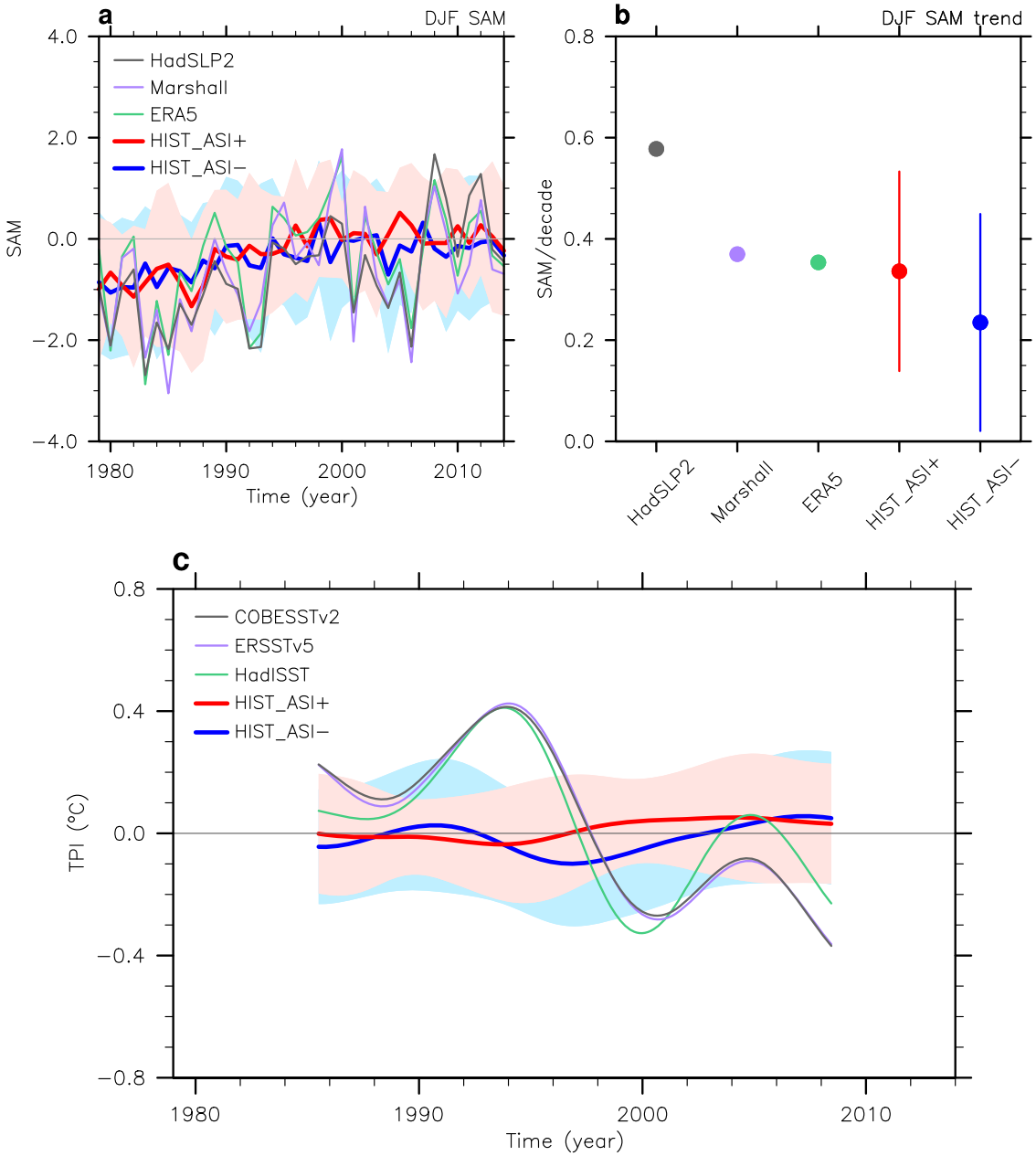

Fig. 7 | Observed and simulated changes in Southern Annual Mode and Interdecadal Pacific Oscillation indices. a The December-January-February (DJF) Southern Annual Mode (SAM) index over 1979–2014 based on HadSLP2 (gray), ERA5 (green), station-based data by Marshall (purple), HIST_ASI+ (ensemble mean, red; ensemble spread, light red), and HIST_ASI- (ensemble mean, blue; ensemble spread, light blue) where the ensemble spread is calculated as one standard deviation among ensembles. **b** Linear trends of the DJF SAM index over 1979–2014 for the same data, using the same color scheme, with dots representing ensemble mean and bars representing ensemble spread for either HIST_ASI+ or HIST_ASI-. **c** The TPI index over 1979-2014 based on COBESSTv2 (gray), ERSSTv5 (purple), HadISST (green), HIST_ASI+ (ensemble mean, red; ensemble spread, light red), and HIST_ASI- (ensemble mean, blue; ensemble spread, light blue). The ensemble spread in HIST_ASI+ or HIST_ASI- is calculated as one standard deviation among ensembles. A 13-year Lanczos filtering has been applied for all the Interdecadal Pacific Oscillation (IPO) timeseries.

In addition, I examine the observed subsurface temperature trend between 1979 and 2014 using the average of EN4, IAP, and Ishii ocean temperature analyses[55–57]. All three sets of data are collected monthly. EN4 data from version 4.2.2 have a horizontal resolution of 1° and 42 vertical levels over a full-depth ocean. They are available in four versions of correction schemes, and I use the average of the four to represent the EN4 data. IAP data from version 3 have a horizontal resolution of 1° and 41 vertical levels in the upper 2000 m. Ishii data from version 7.3.1 have a horizontal resolution of 1° and 28 vertical levels in the upper 3000 m.

I employ the average of GISTEMP, HadCRUT and NOAAGlobalTEMP data[58–60] between 1979 and 2014 to study the observed SAT trend during this period. All three sets of data are collected monthly. GISTEMP data are of the version 4 and have a horizontal resolution of 2°. HadCRUT data are of the version 5.0.2.0 and have a horizontal resolution of 5°, while NOAAGlobalTemp data are of the version of 5.1.0 and have a horizontal resolution of 5°. I also look into the observed precipitation trend between 1979 and 2014 by averaging CMAP, GPCP v2.3, and NOAA's Precipitation Reconstruction (PREC) data[61–63]. All three data are monthly and have a horizontal resolution of 2.5°.

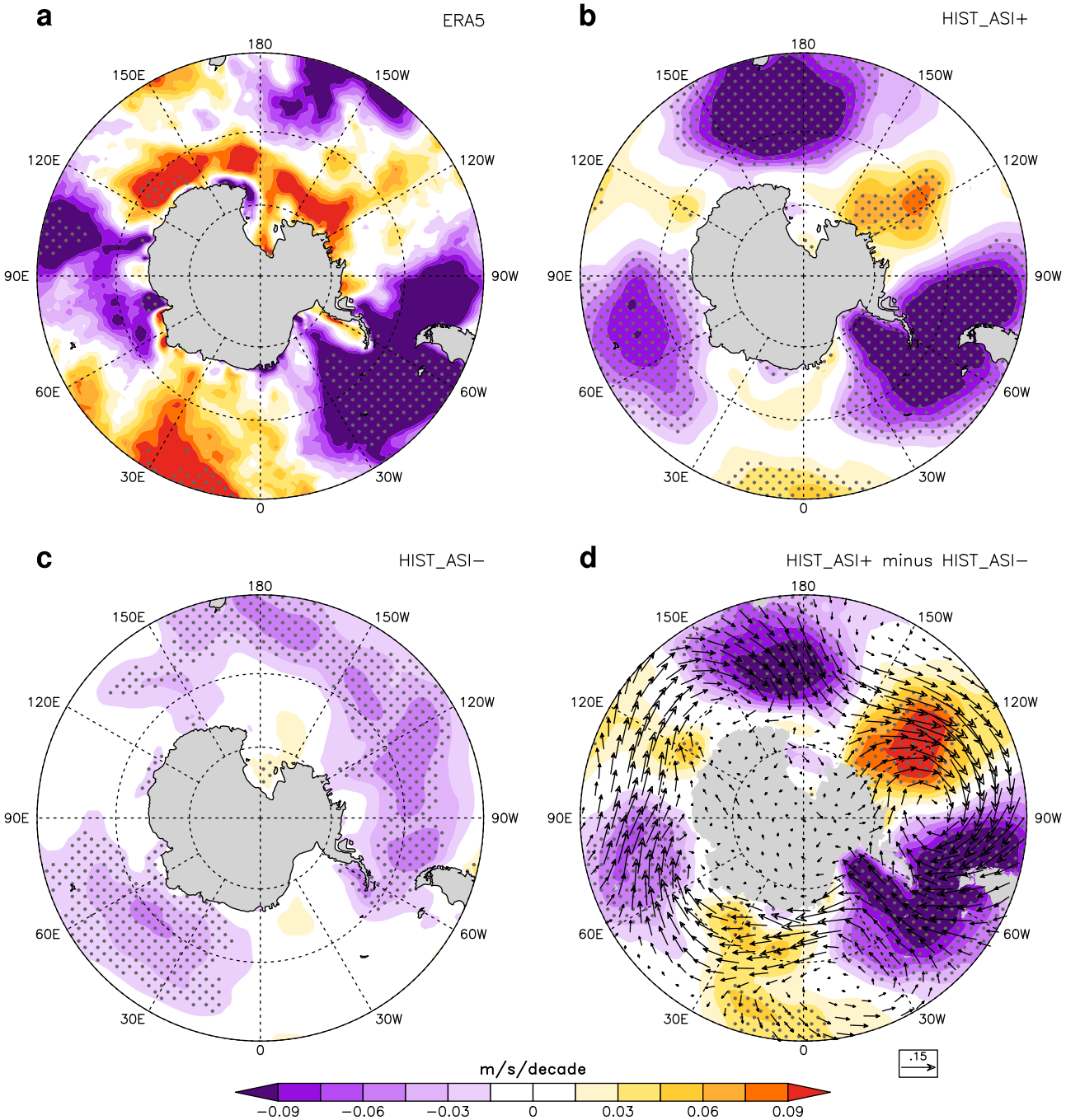

Fig. 8 | Observed and simulated changes in 10-m wind. Linear trends of annual mean 10-m meridional winds over 1979–2014 (color shading in m/s/decade) from (**a**) ERA5, (**b**) HIST_ASI+ and (**c**) HIST_ASI- ensemble means as well as (**d**) the difference between the two (HIST_ASI+ minus HIST_ASI-). The linear trend of annual mean 10-m winds (vector in m/s/decade) during this period is overlapped on (**d**) for the difference between HIST_ASI+ and HIST_ASI- ensemble means. The stipples refer to the regions where trends are statistically significant based on Student's t-test at 95% confidence level.

I use monthly ERA5 reanalysis data[64] between 1979 and 2014 to investigate the observed atmospheric temperature and wind trends during this period. The ERA5 data are organized on a 31-km grid, with 137 levels ranging from the surface to 80 km in height. I further calculate the SAM index[65], which is defined as

$$\mathrm{SAM} = P^*_{40^\circ\mathrm{S}} - P^*_{65^\circ\mathrm{S}} \quad (1)$$

where $P^*_{40°S}$ and $P^*_{65°S}$ are the normalized monthly zonal mean sea level pressures at 40°S and 65°S from 1978 to 2014. I calculate the DJF SAM index from December 1978 to February 2014 using both ERA5 and HadSLP2 data[66], with the latter having a horizontal resolution of 5°. Additionally, I adopt the station-based DJF SAM index by ref. 41 during the same period.

Climate model simulations

I leverage two CMIP5 climate models (GFDL-CM3 and GFDL-ESM2M) and four CMIP6 models (ACCESS-ESM1-5, CAMS-CAM1-0, MIROC6, and MIROC-ES2L) (Table S1). For CMIP5 models, I consider both historical simulations (up to 2005) and Representative Concentration Pathway 8.5 (RCP8.5, after 2005) simulations. For CMIP6 models, I examine their historical simulations. For the sake of simplicity, I refer to these CMIP5/6 simulations as historical simulations. Variables used in the current study

are available for all models, with the exception of some variables that are unavailable in one model (Table S2). I categorize CMIP5/6 historical simulation ensembles based on the trends of their annual mean Antarctic sea ice area from 1979 to 2014: those with significant positive trends ($p < 0.05$) are grouped as HIST_ASI +, totaling 24 ensembles, and those with significant negative trends ($p < 0.05$) are grouped as HIST_ASI-, totaling 53 ensembles (Table S1). I also discover that HIST_ASI+ and HIST_ASI- exhibit distinct evolution patterns of Antarctic sea ice not only in the annual mean but also across seasons (Fig. S2). Importantly, the HIST_ASI+ and HIST_ASI- ensembles are based on the same models, so comparing HIST_ASI+ and HIST_ASI- helps eliminate most of the influence of different model physics. The difference between HIST_ASI+ and HIST_ASI- stems from natural variability, as both are driven by the same external forcings, such as stratospheric ozone depletion and greenhouse gas increases, which facilitates the investigation of the physical processes associated with Antarctic sea ice expansion. Although ensemble-mean results of HIST_ASI+ and HIST_ASI- are mostly discussed in the text, the reflected characteristics, such as sea-ice related SST changes, are robust across models (Fig. S3, S4).

The atmospheric energy-flux theory

According to the atmospheric energy-flux theory[35–40], the location of the zonal mean ITCZ is anticorrelated with atmospheric cross-equatorial energy transport (AET_{EQ}). Given the temporal change of atmospheric energy is neglectable on decadal or longer timescales, AET_{EQ} is determined by the differences of the hemispherical integrations of energy fluxes at the TOA and the ocean/land surface between the Southern Hemisphere and Northern Hemisphere. In particular,

$$AET_{EQ} = \frac{1}{2}\left[\int_{-\pi/2}^{0}\int_{0}^{2\pi}(F_{TOA} - F_{SFC})a^2\cos(\phi')d\lambda d\phi' - \int_{0}^{\pi/2}\int_{0}^{2\pi}(F_{TOA} - F_{SFC})a^2\cos(\phi')d\lambda d\phi'\right] \quad (2)$$

where ϕ', λ and a denote latitude, longitude and the radius of Earth, F_{TOA} and F_{SFC} denote energy fluxes at the TOA and the ocean/land surface, respectively.

Statistical significance test

I conduct the Student's t-test to determine the statistical significance of the linear trend and calculate the p-value to see if it differs significantly from a zero trend.

Data availability

GDFL-CM3 and GFSL-ESM2M data are available at Multi-Model Large Ensemble Archive (MMLEA) https://www.cesm.ucar.edu/community-projects/mmlea, and CMIP6 data are available at https://esgf-node.llnl.gov/projects/cmip6/. The COBE-SSTv2 data are available at https://ds.data.jma.go.jp/tcc/tcc/products/elnino/cobesst2_doc.html. The ERSSTv5 data are available at https://www.ncei.noaa.gov/products/extended-reconstructed-sst. The HadISST data are available at https://www.metoffice.gov.uk/hadobs/hadisst/. The EN4 (version 4.2.2) data are available at http://www.metoffice.gov.uk/hadobs/en4/index.html The IAP data are available at http://www.ocean.iap.ac.cn/. The data from the research led by Ishii (version 7.3.1) are available at https://climate.mri-jma.go.jp/pub/ocean/ts/v7.3.1/temp/. The HadCRUT5 data are available at https://www.metoffice.gov.uk/hadobs/hadcrut5/. The NOAAGlobalTemp data are available at https://www.ncei.noaa.gov/products/land-based-station/noaa-global-temp. The GISTEMP data are available at https://data.giss.nasa.gov/gistemp/. The CMAP precipitation data are available at https://www.cpc.ncep.noaa.gov/products/global_precip/html/wpage.cmap.html. The GPCPv2.3 precipitation data are available at https://psl.noaa.gov/data/gridded/data.gpcp.html. The NOAA's Precipitation Reconstruction (PREC) data are available at https://psl.noaa.gov/data/gridded/data.prec.html. The HadSLP2 data are available at https://www.metoffice.gov.uk/hadobs/hadslp2/. The ERA5 reanalysis data are available at https://www.ecmwf.int/en/forecasts/dataset/ecmwf-reanalysis-v5. The data of station-based SAM index by ref. 36 are available at https://legacy.bas.ac.uk/met/gjma/sam.html.

Code availability

Figures are generated via the NCAR Command Language (NCL, Version 6.5.0) [Software]. (2018). Boulder, Colorado: UCAR/NCAR/CISL/TDD (https://doi.org/10.5065/D6WD3XH5).

Received: 21 August 2024; Accepted: 17 December 2024;
Published online: 07 January 2025

References

1. Comiso, J. C. & Nishio, F. Trends in the sea ice cover using enhanced and compatible AMSR-E, SSM/I, and SMMR data. *J. Geophys Res Oceans* **113**, C02S07 (2008).
2. Bintanja, R., van Oldenborgh, G. J., Drijfhout, S., Wouters, B. & Katsman, C. Important role for ocean warming and increased ice-shelf melt in Antarctic sea-ice expansion. *Nat. Geosci.* **6**, 376–379 (2013).
3. Pauling, A. G., Bitz, C. M., Smith, I. J. & Langhorne, P. J. The response of the Southern Ocean and Antarctic sea ice to freshwater from ice shelves in an Earth system model. *J. Clim.* **29**, 1655–1672 (2016).
4. Rye, C. D. et al. Antarctic glacial melt as a driver of recent Southern Ocean climate trends. *Geophys Res Lett.* **47**, e2019GL086892 (2020).
5. Ferreira, D., Marshall, J., Bitz, C. M., Solomon, S. & Plumb, A. Antarctic Ocean and sea ice response to ozone depletion: A two-time-scale problem. *J. Clim.* **28**, 1206–1226 (2015).
6. Polvani, L. M. et al. Interannual SAM modulation of Antarctic sea ice extent does not account for its long-term trends, pointing to a limited role for ozone depletion. *Geophys Res Lett.* **48**, e2021GL094871 (2021).
7. Chung, E.-S. et al. Antarctic sea-ice expansion and Southern Ocean cooling linked to tropical variability. *Nat. Clim. Change* **12**, 461–468 (2022).
8. Schneider, D. P. & Deser, C. Tropically driven and externally forced patterns of Antarctic sea ice change: Reconciling observed and modeled trends. *Clim. Dyn.* **50**, 4599–4618 (2018).
9. Meehl, G. A., Arblaster, J. M., Bitz, C. M., Chung, C. T. Y. & Teng, H. Antarctic sea-ice expansion between 2000 and 2014 driven by tropical Pacific decadal climate variability. *Nat. Geosci.* **9**, 590–595 (2016).
10. Li, X., Holland, D. M., Gerber, E. P. & Yoo, C. Impacts of the north and tropical Atlantic Ocean on the Antarctic Peninsula and sea ice. *Nature* **505**, 538–542 (2014).
11. Zhang, L., Delworth, T. L., Cooke, W. & Yang, X. Natural variability of Southern Ocean convection as a driver of observed climate trends. *Nat. Clim. Change* **9**, 59–65 (2019).
12. Turner, J. et al. Unprecedented springtime retreat of Antarctic sea ice in 2016. *Geophys Res Lett.* **44**, 6868–6875 (2017).
13. Eayrs, C., Li, X., Raphael, M. N. & Holland, D. M. Rapid decline in Antarctic sea ice in recent years hints at future change. *Nat. Geosci.* **14**, 460–464 (2021).
14. Armour, K. C., Marshall, J., Scott, J. R., Donohoe, A. & Newsom, E. R. Southern Ocean warming delayed by circumpolar upwelling and equatorward transport. *Nat. Geosci.* **9**, 549–554 (2016).
15. Wills, R. C., Dong, Y., Proistosecu, C., Armour, K. C. & Battisti, D. S. Systematic climate model biases in the large-scale patterns of recent sea-surface temperature and sea-level pressure change. *Geophys Res Lett.* **49**, e2022GL100011 (2022).
16. Zhang, L. et al. Roles of meridional overturning in subpolar Southern Ocean SST trends: insights from ensemble simulations. *J. Clim.* **35**, 1577–1596 (2022).
17. Dong, Y., Polvani, L. M. & Bonan, D. B. Recent Multi-Decadal Southern Ocean Surface Cooling Unlikely Caused by Southern Annular Mode Trends. *Geophys Res Lett.* **50**, e2023GL106142 (2023).

18. Zhang, X., Deser, C. & Sun, L. Is there a tropical response to recent observed Southern Ocean cooling? *Geophys Res Lett.* **48**, e2020GL091235 (2021).
19. Dong, Y., Armour, K. C., Battisti, D. S. & Blanchard-Wrigglesworth, E. Two-way teleconnections between the Southern Ocean and the tropical Pacific via a dynamic feedback. *J. Clim.* **35**, 6267–6282 (2022).
20. Kang, S. M. et al. Global impacts of recent Southern Ocean cooling. *Proc. Natl Acad. Sci. USA* **120**, e2300881120 (2023).
21. Turner, J., Bracegirdle, T. J., Phillips, T., Marshall, G. J. & Hosking, J. S. An initial assessment of Antarctic sea ice extent in the CMIP5 models. *J. Clim.* **26**, 1473–1484 (2013).
22. Roach, L. A. et al. Antarctic sea ice area in CMIP6. *Geophys Res Lett.* **47**, e2019GL086729 (2020).
23. Andrews, T. et al. Accounting for changing temperature patterns increases historical estimates of climate sensitivity. *Geophys Res Lett.* **45**, 8490–8499 (2018).
24. Blanchard-Wrigglesworth, E., Roach, L. A., Donohoe, A. & Ding, Q. Impact of winds and Southern Ocean SSTs on Antarctic sea ice trends and variability. *J. Clim.* **34**, 949–965 (2021).
25. Schmidt, G. A. et al. Anomalous meltwater from ice sheets and ice shelves is a historical forcing. *Geophys Res Lett.* **50**, e2023GL106530 (2023).
26. Roach, L. A. et al. Winds and meltwater together lead to Southern Ocean surface cooling and sea ice expansion. *Geophys Res Lett.* **50**, e2023GL105948 (2023).
27. Sun, S. & Eisenman, I. Observed Antarctic sea ice expansion reproduced in a climate model after correcting biases in sea ice drift velocity. *Nat. Comm.* **12**, 1060 (2021).
28. Rackow, T. et al. Delayed Antarctic sea-ice decline in high-resolution climate change simulations. *Nat. Comm.* **13**, 637 (2022).
29. Singh, H. A., Polvani, L. M. & Rasch, P. J. Antarctic sea ice expansion, driven by internal variability, in the presence of increasing atmospheric CO2. *Geophys Res Lett.* **46**, 14762–14771 (2019).
30. Polvani, L. M. & Smith, K. L. Can natural variability explain observed Antarctic sea ice trends? New modeling evidence from CMIP5. *Geophys Res Lett.* **40**, 3195–3199 (2013).
31. Haumann, F. A., Gruber, N. & Münnich, M. Sea-ice induced Southern Ocean subsurface warming and surface cooling in a warming climate. *AGU Adv.* **1**, e2019AV000132 (2020).
32. Zhang, L. et al. The relative role of the subsurface Southern Ocean in driving negative Antarctic Sea ice extent anomalies in 2016–2021. *Commun. Earth Environ.* **3**, 302 (2022).
33. England, M. R., Polvani, L. M., Sun, L. & Deser, C. Tropical climate responses to projected Arctic and Antarctic sea-ice loss. *Nat. Geosci.* **13**, 275–281 (2020).
34. Chadwick, R., Boutle, I. & Martin, G. Spatial patterns of precipitation change in CMIP5: Why the rich do not get richer in the tropics. *J. Clim.* **26**, 3803–3822 (2013).
35. Kang, S. M., Held, I. M., Frierson, D. M. & Zhao, M. The response of the ITCZ to extratropical thermal forcing: Idealized slab-ocean experiments with a GCM. *J. Clim.* **21**, 3521–3532 (2008).
36. Schneider, T., Bischoff, T. & Haug, G. H. Migrations and dynamics of the intertropical convergence zone. *Nature* **513**, 45–53 (2014).
37. Liu, W. & Hu, A. The role of the PMOC in modulating the deglacial shift of the ITCZ. *Clim. Dyn.* **45**, 3019–3034 (2015).
38. Liu, W. & Fedorov, A. V. Global impacts of Arctic sea ice loss mediated by the Atlantic meridional overturning circulation. *Geophys Res Lett.* **46**, 944–952 (2019).
39. Li, S. & Liu, W. Deciphering the migration of the intertropical convergence zone during the last deglaciation. *Geophys Res Lett.* **49**, e2022GL098806 (2022).
40. Liu, W., Li, S., Li, C., Rugenstein, M. & Thomas, A. P. Contrasting fast and slow intertropical convergence zone migrations linked to delayed Southern Ocean warming. *Nat. Clim. Change* **14**, 732–739 (2024).
41. Marshall, G. J. Trends in the Southern Annular Mode from observations and reanalyses. *J. Clim.* **16**, 4134–4143 (2003).
42. Swart, N. C. & Fyfe, J. C. Observed and simulated changes in the Southern Hemisphere surface westerly wind-stress. *Geophys Res Lett.* **39**, L16711 (2012).
43. Meehl, G. A., Teng, H. & Arblaster, J. M. Climate model simulations of the observed early-2000s hiatus of global warming. *Nat. Clim. Change* **4**, 898–902 (2014).
44. Lefebvre, W., Goosse, H., Timmermann, R. & Fichefet, T. Influence of the Southern Annular Mode on the sea ice–ocean system. *J. Geophys. Res. Oceans* **109**, C09005 (2004).
45. Holland, P. R. & Kwok, R. Wind-driven trends in Antarctic sea-ice drift. *Nat. Geosci.* **5**, 872–875 (2012).
46. Haumann, F. A., Notz, D. & Schmidt, H. Anthropogenic influence on re- cent circulation-driven Antarctic sea ice changes. *Geophys Res Lett.* **41**, 8429–8437 (2014).
47. Turner, J., Hosking, J. S., Marshall, G. J., Phillips, T. & Bracegirdle, T. J. Antarctic sea ice increase consistent with intrinsic variability of the Amundsen Sea Low. *Clim. Dyn.* **46**, 2391–2402 (2016).
48. van Loon, H. & Jenne, R. L. The zonal harmonic standing waves in the Southern Hemisphere. *J. Geophys Res.* **77**, 992–1003 (1972).
49. Eabry, M., Goyal, R., Taschetto, A., Hobbs, W. & Sen Gupta, A. Combined Impacts of Southern Annular Mode and Zonal Wave Three on Antarctic Sea Ice Variability. *J. Clim.* **37**, 1759–1775 (2024).
50. Cavalieri, D. J., Gloersen, P. & Campbell, W. J. Determination of sea ice parameters with the Nimbus 7 SMMR. *J. Geophys Res* **89**, 5355–5369 (1984).
51. Hirahara, S., Ishii, M. & Fukuda, Y. Centennial-scale sea surface temperature analysis and its uncertainty. *J. Clim.* **27**, 57–75 (2014).
52. Huang, B. et al. Extended reconstructed sea surface temperature, version 5 (ERSSTv5): upgrades, validations, and intercomparisons. *J. Clim.* **30**, 8179–8205 (2017).
53. Rayner, N. A. et al. Global analyses of sea surface temperature, sea ice, and night marine air temperature since the late nineteenth century. *J. Geophys Res Atmos.* **108**, 4407 (2003).
54. Henley, B. J. et al. A Tripole Index for the Interdecadal Pacific Oscillation. *Clim. Dyn.* **45**, 3077–3090 (2015).
55. Good, S. A., Martin, M. J. & Rayner, N. A. EN4: quality controlled ocean temperature and salinity profiles and monthly objective analyses with uncertainty estimates. *J. Geophys Res Oceans* **118**, 6704–6716 (2013).
56. Cheng, L. et al. Improved estimates of ocean heat content from 1960 to 2015. *Sci. Adv.* **3**, e1601545 (2017).
57. Ishii, M., Shouji, A., Sugimoto, S. & Matsumoto, T. Objective analyses of SST and marine meteorological variables for the 20th century using COADS and the Kobe Collection. *Int J. Climatol.* **25**, 865–879 (2005).
58. Lenssen, N. G. et al. Improvements in the GISTEMP uncertainty model. *J. Geophys Res Atmos.* **124**, 6307–6326 (2019).
59. Morice, C. P. et al. An updated assessment of near-surface temperature change from 1850: the HadCRUT5 dataset. *J. Geophys Res Atmos.* **126**, e2019JD032361 (2021).
60. Huang, B. et al. Uncertainty estimates for sea surface temperature and land surface air temperature in NOAAGlobalTemp version 5. *J. Clim.* **33**, 1351–1379 (2020).
61. Xie, P. & Arkin, P. A. Global precipitation: a 17-year monthly analysis based on gauge observations, satellite estimates, and numerical model outputs. *Bull. Am. Meteor Soc.* **78**, 2539–2558 (1997).
62. Adler, R. et al. The Global Precipitation Climatology Project (GPCP) Monthly Analysis (New Version 2.3) and a Review of 2017 Global Precipitation. *Atmosphere* **9**, 138 (2018).
63. Chen, M., Xie, P., Janowiak, J. E. & Arkin, P. A. Verifying the reanalysis and climate models outputs using a 56-year data set of reconstructed global precipitation. 14th AMS Conf Appl Meteor 11-15 January, 2004, Seattle, WA (2004).

64. Hersbach, H. et al. The ERA5 global reanalysis. *Q J. R. Meteorol. Soc.* **146**, 1999–2049 (2020).
65. Gong, D. & Wang, S. Definition of Antarctic oscillation index. *Geophys Res Lett.* **26**, 459–462 (1999).
66. Allan, R. & Ansell, T. A new globally complete monthly historical gridded mean sea level pressure dataset (HadSLP2): 1850-2004. *J. Clim.* **22**, 5816–5842 (2006).

Acknowledgements

This study has been supported by U.S. National Science Foundation (OCE-2123422, AGS-2053121, and AGS-2237743).

Author contributions

W.L. conceived the study, performed the analysis, wrote the manuscript text and prepared figures 1-8.

Competing interests

The author declares no competing interests.

Additional information

Supplementary information The online version contains supplementary material available at https://doi.org/10.1038/s41612-024-00881-1.

Correspondence and requests for materials should be addressed to Wei Liu.